

Dalton Transactions

Accepted Manuscript



This is an *Accepted Manuscript*, which has been through the Royal Society of Chemistry peer review process and has been accepted for publication.

Accepted Manuscripts are published online shortly after acceptance, before technical editing, formatting and proof reading. Using this free service, authors can make their results available to the community, in citable form, before we publish the edited article. We will replace this *Accepted Manuscript* with the edited and formatted *Advance Article* as soon as it is available.

You can find more information about *Accepted Manuscripts* in the [Information for Authors](#).

Please note that technical editing may introduce minor changes to the text and/or graphics, which may alter content. The journal's standard [Terms & Conditions](#) and the [Ethical guidelines](#) still apply. In no event shall the Royal Society of Chemistry be held responsible for any errors or omissions in this *Accepted Manuscript* or any consequences arising from the use of any information it contains.

ARTICLE

Slow magnetic relaxation of light lanthanide-based linear LnZn₂ trinuclear complexes

Cite this: DOI: 10.1039/x0xx00000x

Chika Takehara,^a Poh Ling Then,^a Yumiko Kataoka,^a Motohiro Nakano,^b Tomoo Yamamura,^c and Takashi Kajiwara^{*a}Received 00th January 2012,
Accepted 00th January 2012

DOI: 10.1039/x0xx00000x

www.rsc.org/

Four isostructural LnZn₂ trinuclear complexes, [Ln(NO₃){Zn(L)(SCN)}₂] (H₂L is a Schiff base ligand derived from *o*-vanillin and ethylenediamine), were synthesized, which include light lanthanide ions as spin carriers (Ln = Ce **1**, Pr **2**, Nd **3**, and Sm **4**). These complexes involve a linear Zn(II)–Ln(III)–Zn(II) array, which leads to an axially stressed ligand field and can also cause single-molecule magnet (SMM) behavior in oblate-type electronic distributions of ground sublevels found in Ce(III), Pr(III), and Nd(III). Slow magnetic relaxation behavior was observed in **1** and **3** under an applied bias dc field of 1000 Oe, whereas such a slow relaxation was not observed in **2** and **4**. The appearance of field-induced SMM behavior in **1** and **3** was correlated with the even-numbered J_z sublevels of Ce(III) and Nd(III) ions known as the Kramers system.

Introduction

Single-molecule magnets (SMMs)¹ are one of the most fascinating materials in the field of molecule-based nanomaterials. SMMs exhibit slow magnetic relaxation originating from the combination of a large angular momentum and large easy-axis magnetic anisotropy. For designing better SMMs, heavy lanthanide (Ln) ions such as Tb(III) and Dy(III) are assumed to be advantageous^{2–9} because of their large magnetic momentum J (defined as $J = S + L$, where S denotes the spin angular momentum and L denotes the orbital angular momentum). The expected J values are 6 and 15/2 for Tb(III) and Dy(III), respectively. When Ln(III) is surrounded by an anisotropic environment, the degeneracy of the J state is lost and isolated sublevels are formed. These sublevels can be distinguished by the quantum number J_z when the coordination anisotropy is weak and of an axial type. If the Ln(III) ion is located in an appropriate anisotropy during coordination, the highest $|J_z|$ sublevels stabilize and separate from the 1st excited sublevels with the separation being large enough to prevent the reversal of magnetization. The situation is similar to that of light lanthanide ions,¹⁰ however, smaller separations would be expected because of the smaller total angular momentum defined as $J = |S - L|$.

As was reported previously, each $|J_z|$ sublevel of the lanthanide ions has differently shaped electronic distributions.¹¹ The negatively charged set of donor atoms affects each $|J_z|$ sublevel in a different way as a different anisotropic electrostatic field.¹² In previous studies,³ we have demonstrated the relationship between the geometry of the crystal field and the magnetic anisotropy of several heavy Ln(III) SMMs, along with Ce(III) SMMs,^{3b,3c} that are synthesized in a manner similar to that of Tb(III) SMMs. The Tb(III) ion has an f^8 configuration, and its 13-fold 7F_6 ground state splits into 7 sets of Kramers pairs, characterized by $|J_z|$. The highest $|J_z|$ sublevels with $|J_z| =$

6 are known to have an oblate spheroidal (or “pound-cake”-shaped) electronic distribution,^{11,12} whereas the $J_z = 0$ sublevel has a prolate distribution along the principle axis. Hence, Tb(III) is known as an oblate-type ion. The light lanthanide Ce(III) is also an oblate-type ion, having the same orbital angular momentum and similar $^2F_{5/2}$ ground multiplet as Tb(III). It is also similar to, albeit slightly more complicated than, Nd(III) with a $^4I_{9/2}$ ground state. If the crystal field is designed such that the highest $|J_z|$ sublevels are more stabilized than the other sublevels, an easy-axis anisotropy that realizes slow magnetic relaxation is introduced.¹² We have reported the SMM features of linear trinuclear Zn(II)–Ln(III)–Zn(II) complexes formulated as [Ln(NO₃){Zn(L)(SCN)}₂] (H₂L denotes a Schiff base ligand derived from *o*-vanillin and ethylenediamine in a 1:2 ratio; Ln(III) = Tb(III) and Dy(III)), in which the Ln(III) ion is sandwiched between two sets of two phenoxo oxygen donors along the Zn(II)–Ln(III)–Zn(II) axis.^{3a} From the DFT calculation, we have found that the Mulliken charges of the phenoxo oxygen atoms are larger than those of methoxy and nitrate oxygen donors,³¹ and hence, Ln(III) ions are located in an axially anisotropic ligand field. This leads to easy-axis magnetic anisotropy and SMM features of Tb(III) and Dy(III) complexes. As Ce(III) and Nd(III) are oblate-type ions, similar trinuclear complexes would lead to SMM features of which the correlation between coordination anisotropy and appearance of slow magnetic relaxation phenomena could be discussed from a magnetostructural viewpoint. Hence, we have synthesized a series of isostructural complexes with Ln(III) = Ce(III) **1**, Pr(III) **2**, Nd(III) **3**, and Sm(III) **4** that are also isostructural with previously reported La(III) complexes, as well as Tb(III) and Dy(III) SMMs. The crystal structures of **1–4** and the detailed SMM features of **1** and **3** are reported herein.

Experimental

All chemicals and reagents were of reagent grade and were used without further purification. All chemical reactions and sample preparations for physical measurements were performed in air.

Instrumentation

Variable-temperature magnetic susceptibility measurements were performed on MPMS-5S and PPMS-9 magnetometers (Quantum Design). Polycrystalline sample and small amount of acetonitrile were sealed into gelatin capsule to avoid the removal of the solvent molecule of the crystallization during the data collection. Diamagnetic corrections for each sample were applied using Pascal's constants. Elemental analysis was carried out with the help of the Research and Analytical Center for Giant Molecules, Graduate School of Science, Tohoku University.

Synthetic procedures

Synthesis of $[\text{Ce}(\text{NO}_3)_3\{\text{Zn}(\text{L})(\text{SCN})_2\}_2]\cdot\text{CH}_3\text{CN}$ (1**· CH_3CN).** Schiff-base ligand H_2L (32.8 mg, 0.1 mmol) was dissolved by heating in acetonitrile (1.5 mL), and a methanolic solution of $\text{Zn}(\text{OAc})_2\cdot 2\text{H}_2\text{O}$ (0.1 mmol), $\text{Ce}(\text{NO}_3)_3\cdot 6\text{H}_2\text{O}$ (0.05 mmol), and tetrabutylammonium thiocyanate (0.1 mmol) was added to the H_2L solution. The mixture was left to stand in an incubator (45°C).

Yellow crystals suitable for X-ray crystallography were obtained after several days. Yield = 39 mg, 68%. Elemental Anal. Calcd. for **1**· CH_3CN C, 42.04; H, 3.44; N, 9.81. Found: C, 41.98; H, 3.43; N, 9.55.

Synthesis of $[\text{Pr}(\text{NO}_3)_3\{\text{Zn}(\text{L})(\text{SCN})_2\}_2]\cdot\text{CH}_3\text{CN}$ (2**· CH_3CN), $[\text{Nd}(\text{NO}_3)_3\{\text{Zn}(\text{L})(\text{SCN})_2\}_2]\cdot\text{CH}_3\text{CN}$ (**3**· CH_3CN) and $[\text{Sm}(\text{NO}_3)_3\{\text{Zn}(\text{L})(\text{SCN})_2\}_2]\cdot\text{CH}_3\text{CN}$ (**4**· CH_3CN).** Complexes **2**, **3** and **4** were also obtained by the same procedure as described above, except that $\text{Pr}(\text{NO}_3)_3\cdot 6\text{H}_2\text{O}$, $\text{Nd}(\text{NO}_3)_3\cdot 6\text{H}_2\text{O}$ and $\text{Sm}(\text{NO}_3)_3\cdot 6\text{H}_2\text{O}$ were used as starting materials for **2**, **3** and **4**, respectively. Yield = 40 mg, 70% for **2**, 42 mg, 73% for **3**, 46 mg, 73% for **4**. Elemental Anal. Calcd. for **2**· CH_3CN C, 42.01; H, 3.44; N, 9.90. Found C, 41.81; H, 3.50; N, 9.63. Calcd. for **3**· CH_3CN C, 41.89; H, 3.43; N, 9.77. Found C, 41.71; H, 3.49; N, 9.51. Calcd. for **4**· CH_3CN C, 41.67; H, 3.41; N, 9.72. Found C, 41.43; H, 3.45; N, 9.45.

Crystallography

X-ray data for **1–4** were collected at a low temperature (153 K) on a Rigaku Varimax Saturn area detector diffractometer using confocal monochromated Mo $K\alpha$ radiation. The intensity data were empirically corrected for absorption by an empirical method included in the Crystal Clear program.^{13a} The structures were solved by direct methods with SIR-97,^{13b} and structure refinement was carried out by full-matrix least-squares on

Table 1 Crystal data for all complexes.

	1 · CH_3CN	2 · CH_3CN	3 · CH_3CN	4 · CH_3CN
Formula	$\text{C}_{40}\text{H}_{39}\text{N}_8\text{O}_{11}\text{S}_2\text{Zn}_2\text{Ce}$	$\text{C}_{40}\text{H}_{39}\text{N}_8\text{O}_{11}\text{S}_2\text{Zn}_2\text{Pr}$	$\text{C}_{40}\text{H}_{39}\text{N}_8\text{O}_{11}\text{S}_2\text{Zn}_2\text{Nd}$	$\text{C}_{40}\text{H}_{39}\text{N}_8\text{O}_{11}\text{S}_2\text{Zn}_2\text{Sm}$
FW	1142.77	1143.56	1146.89	1153.00
Crystal system	Triclinic	Triclinic	Triclinic	Triclinic
Space group	$P\bar{1}$	$P\bar{1}$	$P\bar{1}$	$P\bar{1}$
$a / \text{\AA}$	12.0836(19)	12.0853(11)	12.0855(19)	12.0861(12)
$b / \text{\AA}$	12.587(2)	12.5724(14)	12.552(2)	12.5205(15)
$c / \text{\AA}$	16.363(3)	16.3404(17)	16.340(3)	16.3338(18)
$\alpha / ^\circ$	87.699(8)	87.928(4)	87.999(6)	88.163(5)
$\beta / ^\circ$	69.461(5)	69.558(3)	69.453(5)	69.476(4)
$\gamma / ^\circ$	70.611(6)	70.611(3)	70.683(5)	70.607(3)
$V / \text{\AA}^3$	2190.2(7)	2185.5(4)	2181.0(7)	2173.5(4)
Z	2	2	2	2
$D / \text{g cm}^{-3}$	1.733	1.738	1.746	1.762
T / K	153(2)	153(2)	153(2)	153(2)
Wavelength / \AA	0.71075	0.71075	0.71075	0.71075
$F(000)$	1146	1148	1150	1154
μ / mm^{-1}	2.272	2.350	2.429	2.593
θ range / $^\circ$	2.27–30.00	2.08–30.00	1.73–30.00	1.34–30.00
$R_1, wR_2 (I > 2\sigma(I))$	0.056, 0.140	0.037, 0.088	0.045, 0.094	0.038, 0.087
R_1, wR_2 (all data)	0.062, 0.147	0.043, 0.092	0.055, 0.100	0.044, 0.092

SHELXL-97.^{13c} Nonhydrogen atoms were anisotropically refined, and the hydrogen atoms were treated using a riding model. Table 1 lists the crystallographic data and the R_1 and wR_2 values.

Results and discussion

Synthesis and crystal structures

Trinuclear complexes $[\text{Ln}(\text{NO}_3)\{\text{Zn}(\text{L})(\text{SCN})\}_2]$ were initially synthesized by Jones et al.¹⁴ for $\text{Ln} = \text{Nd}, \text{Eu}, \text{Tb},$ and Er to investigate luminescence properties. We then reported the synthesis and magnetism of such complexes including $\text{Ln} = \text{Tb}$ and Dy .^{3a} These complexes crystallized in two types of isostructural groups showing a slight difference in the $\text{Zn}(\text{II})\text{--}\text{Ln}(\text{III})\text{--}\text{Zn}(\text{II})$ array. One group showed a bend arrangement ($\text{Zn--Ln--Zn} \approx 135^\circ$) that was found in the complexes synthesized with heavier lanthanides such as $\text{Tb}, \text{Dy},$ and Er , whereas the other showed a more linear arrangement ($\text{Zn--Ln--Zn} \approx 168^\circ$) that was found in the complexes synthesized using lighter lanthanides such as La and Eu . For the construction of SMMs using oblate-type lanthanides, the latter structure is preferable to achieve easy-axis type magnetic anisotropy. As was expected for the light lanthanide ions of $\text{Ce}(\text{III}), \text{Pr}(\text{III}), \text{Nd}(\text{III}),$ and $\text{Sm}(\text{III})$, complexes **1–4** were crystallized in an isostructural manner similar to that reported for $\text{La}(\text{III})$. Also, in these complexes, the coordination structures around $\text{Ln}(\text{III})$ were assumed to be suited for easy-axis anisotropy. This was elucidated from X-ray analysis.

Table 1 lists the details of the X-ray crystallographic analysis for complexes **1–4**. All complexes crystallized in the triclinic $P\bar{1}$ space group. Fig. 1 shows the ORTEP drawings and molecular structures of **1**, and Table 2 lists the selected atom...atom distances and angles of **1–4**. The molecular structures of **1** consisted of two mononuclear $\{\text{Zn}(\text{L})(\text{SCN})\}^-$ units that behaved as chelating ligands to Ce via two phenoxo oxygen atoms (O5/O6 or O9/O10) with normal coordination distances (2.457(2)–2.474(2) Å), and via two methoxy oxygen atoms (O4/O7 or O8/O11) with longer coordination distances (2.612(3)–2.789(3) Å). Each Zn in the complex-ligand shows

Table 2 Selected atom...atom distances (Å) and angles ($^\circ$) for **1–4**.

	1·CH₃CN	2·CH₃CN	3·CH₃CN	4·CH₃CN
Ln–O1	2.649(3)	2.639(2)	2.634(3)	2.614(2)
Ln–O2	2.549(3)	2.529(2)	2.511(2)	2.482(2)
Ln–O4	2.789(3)	2.780(2)	2.777(2)	2.784(2)
Ln–O5	2.469(2)	2.4446(18)	2.434(2)	2.4083(19)
Ln–O6	2.474(2)	2.4603(18)	2.444(2)	2.4120(19)
Ln–O7	2.744(3)	2.7347(19)	2.723(2)	2.706(2)
Ln–O8	2.612(3)	2.5981(19)	2.585(2)	2.560(2)
Ln–O9	2.457(2)	2.4381(18)	2.417(2)	2.3857(19)
Ln–O10	2.471(3)	2.4475(18)	2.435(2)	2.4030(18)
Ln–O11	2.694(3)	2.6776(19)	2.668(2)	2.6573(19)
Ln–Zn1	3.6937(8)	3.6769(5)	3.6676(7)	3.6441(5)
Ln–Zn2	3.5763(8)	3.5646(5)	3.5506(8)	3.5247(5)
Ln...Ln ^{#1}	7.9766(15)	7.9793(9)	7.9847(16)	8.0089(9)
Zn1–Ln–Zn2	167.98(1)	168.43(1)	168.77(1)	169.36(1)

Symmetry transformations used to generate equivalent atoms: #1 2–x, 1–y, –z

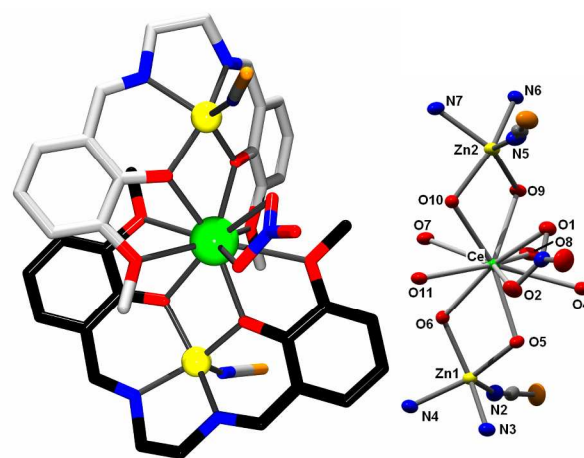


Fig. 1 Molecular structure of **1** (left). ORTEP drawing of the coordination environment around the linear Zn--Ce--Zn array of **1** at 50% probability (right). Hydrogen atoms are omitted for clarity. Green Tb, yellow Zn, orange S, red O, blue N, and gray and black, C.

pentacoordination with a distorted square pyramidal geometry, surrounded by N_2O_2 donor sets from the Schiff base ligand in an equatorial manner and the N atom from SCN^- at the apical position. $\text{Ln}(\text{III})$ exhibited decacoordination, where eight O atoms belong to two complex ligands $\{\text{Zn}(\text{L})(\text{SCN})\}^-$, and two O atoms belong to the bidentate nitrate group [$\text{O1/O2}, 2.649(3)$ and $2.549(3)$ Å]. The Zn1--Ce--Zn2 array was close to linear structure [$167.98(1)^\circ$] and similar to that found in the $\text{La}(\text{III})$ complex [$168.04(1)^\circ$]. Hence, Ce was sandwiched between two sets of phenoxo oxygen atoms along the Zn1--Ce--Zn2 axis. This leads to the large negative charge of the phenoxo oxygen atoms being concentrated above and below Ce. The special arrangement between the two phenoxo oxygen pairs and the f-electron density of $\text{Ln}(\text{III})$ is an important factor to discuss in magnetic anisotropy. In the previous paper, we have defined two structural parameters ϕ and θ , ϕ is the angle between the centers of the phenoxo oxygen pairs ($\text{O}_{\text{Ph}}\cdots\text{O}_{\text{Ph}}$) and $\text{Ln}(\text{III})$ and

it was estimated to be 159.3° , whereas θ is defined as the angle between the vectors of $\text{O}_{\text{Ph}}\cdots\text{O}_{\text{Ph}}$ and it was estimated as 66.9° for **1**. Large ϕ and small θ values are preferable for maximizing the anisotropy of oblate ions such as Ce, since ϕ , with a value close to 180° , results in the negative charges of the donor atoms being located right above and below $\text{Ln}(\text{III})$. Also, a small θ value results in the phenoxo oxygen pairs being parallel to each other. The observed values were differed from the corresponding values; however, they were very close to those found in $\text{Tb}(\text{III})$ -based and $\text{Dy}(\text{III})$ -based SMMs that are isostructural with **1–4**. Slow magnetic relaxation phenomena would be expected for the oblate ions of $\text{Ce}(\text{III}), \text{Pr}(\text{III}),$ and $\text{Nd}(\text{III})$; on the contrary, such an easy-axis anisotropy could not be expected for $\text{Sm}(\text{III})$, which is located at the boundary between the oblate and prolate ions.

The shortest $\text{Ln}\cdots\text{Ln}$ distances were estimated as $7.9766(15)\text{--}8.0089(9)$ Å. This is long enough to avoid the through-space magnetic interactions among $\text{Ln}(\text{III})$ ions in the solid state. In the crystal lattice, the complexes contained a molecule of acetonitrile as the solvent of crystallization.

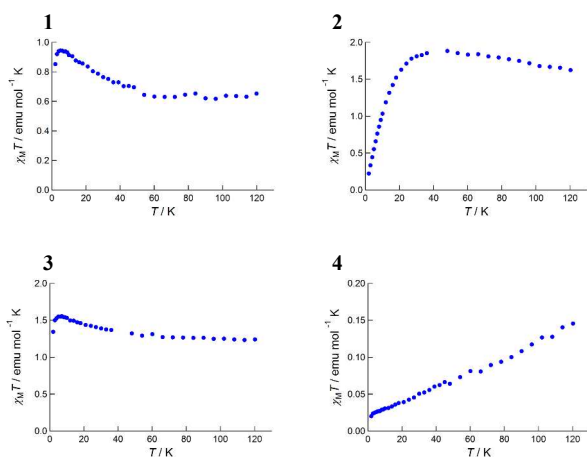


Fig. 2 Temperature dependence of products of molar susceptibility χ_M and temperature T of complexes 1–4.

Magnetic properties

Dc susceptibility data were recorded at variable temperatures (below 120 K) for all complexes under the application of a dc field of 1000 Oe. Fig. 2 shows the temperature dependence of $\chi_M T$ products. The $\chi_M T$ values of complexes 2 and 4 exhibited a strong temperature dependence. For 4, it linearly decreased over the whole temperature range. For 2, $\chi_M T$ value first increased during the cooling, and below 30 K, it abruptly decreased toward the value of 0 emu K mol⁻¹. The Curie constants for Ln in an isotropic ligand field were estimated to be 1.60 emu K mol⁻¹ for Pr(III) ($S = 1$, $L = 5$, $J = 4$, $g = 4/5$) and 0.089 emu K mol⁻¹ for Sm(III) ($S = 5/2$, $L = 5$, $J = 5/2$, $g = 2/7$). The highest $\chi_M T$ value observed above was similar to (for Pr(III)), or larger than (for Sm(III)), these values. A strong temperature dependence at low temperature region, attributed to the thermal depopulation among J_z sublevels split under the anisotropic ligand field, was common to these lanthanide complexes. On the contrary, the $\chi_M T$ values of complexes 1 and 3 exhibited a weaker temperature dependence for the entire temperature range. The values slightly increased when samples were cooled down to 5 K, and then decreased when the temperature was further cooled below 5 K. The maximum $\chi_M T$ values were 0.93 and 1.6 emu K mol⁻¹, respectively. These were close to the Curie constants of 0.80 emu K mol⁻¹ for Ce(III) ($S = 1/2$, $L = 3$, $J = 5/2$, $g = 6/7$) and 1.64 emu K mol⁻¹ for Nd(III) ($S = 1$, $L = 5$, $J = 4$, $g = 4/5$). The exact values of $\chi_M T$ for these complexes do not give much information, however, the difference of the temperature dependence of $\chi_M T$ is highly suggestive especially at low temperature, since slow magnetic relaxation phenomena are observed below 20 K or lower. 1 and 3 exhibited the highest $\chi_M T$ values in this region. Accompanied by their weak temperature-dependent behavior, observation for 1 and 3 could be understood by assuming that the large $|J_z|$ ground sublevels of Ce(III) in 1 and Nd(III) in 3 are sufficiently separated from other excited sublevels and are mainly occupied at a low temperature range below 10 K.

The slow magnetic relaxation features of the complexes were confirmed by measuring the alternating current (ac) magnetic susceptibility initially recorded under zero dc fields (Fig. 3). None of the complexes exhibited any out-of-phase signals, χ_M'' , under these conditions. The products of the in-phase signals and

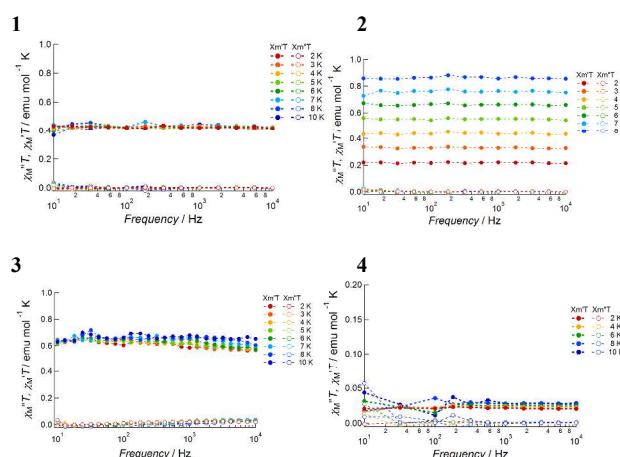


Fig. 3 Frequency dependence of products $\chi_M' T$ (closed circle) and $\chi_M'' T$ (open circle) of 1–4 measured under an oscillating field of 3 Oe and zero dc field.

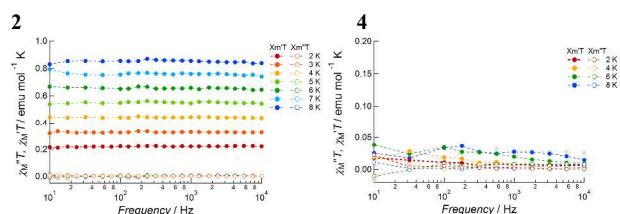


Fig. 4 Frequency dependence of products $\chi_M' T$ (closed circle) and $\chi_M'' T$ (open circle) of 2 and 4 measured under an oscillating field of 3 Oe and an applied 1000 Oe dc field.

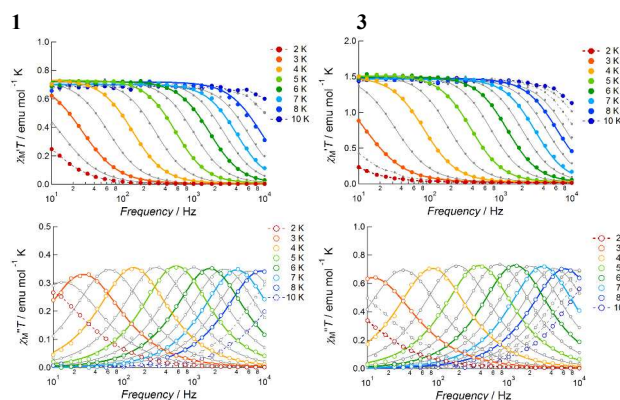


Fig. 5 Frequency dependence of products $\chi_M' T$ (top, closed circle) and $\chi_M'' T$ (bottom, open circle) of 1 (left) and 3 (right) measured under an oscillating field of 3 Oe and an applied 1000 Oe dc field. Solid curves represent the theoretical calculation on the basis of the generalized Debye model whereas dashed curves are visual guides.

temperature, $\chi_M' T$, were independent of the ac field frequency, and showed different temperature dependences between the 1 and 3 pair, and 2. The $\chi_M' T$ values for 1 and 3 were almost independent of the temperature at a range between 2 K and 10 K, and exhibited Curie-like behavior. On the other hand, $\chi_M' T$ products of 2 showed a strong temperature dependence that increased linearly with an increase in temperature. This observation may be due to the presence of thermal depopulation among J_z sublevels split under an anisotropic ligand field. With

the application of a dc bias field of 1000 Oe, **2** and **4** maintained their paramagnetic features. This was similar to their behavior under zero field conditions (Fig. 4). On the contrary, **1** and **3** exhibited out-of-phase signals which were observed at temperatures up to 8 K and 9 K, respectively (ac frequency of 10000 Hz, Fig. 5). This was indicative of the presence of slow magnetic relaxation.

Bias field dependence of the slow relaxation in **1** was revealed at a field range of 0–1000 Oe for a temperature range of 2–8 K (Figs. S1 and S2). With the application of a dc field, there was a slight increase in the amplitude of susceptibility of **1** with a simultaneous observation of frequency-dependent out-of-phase signals. The appearance of the out-of-phase signals accompanied by a decrease in the adiabatic susceptibility of χ_S indicates that fast tunneling relaxation is dominant under zero field conditions, which was suppressed by applying a bias dc field. The amplitude of $\chi_M''T$ is very sensitive to the magnitude of the weak dc field; it increased when a weak field of 25–100 Oe was applied, and reached a constant value when the field was above 500 Oe. This occurred along with the disappearance of $\chi_S T$. A similar field-dependent slow magnetic relaxation has been observed for the Ce(III) SMMs.^{3b,3c} These relaxation phenomena obeyed Debye relaxation. The frequency dependence of both the in-phase and out-of-phase signals were well fitted with the generalized Debye equations using four parameters namely, isothermal susceptibility χ_T , adiabatic susceptibility χ_S , relaxation time τ , and distribution of τ , α (the four parameters are summarized in Table S1 for the case of an applied 1000 Oe dc field). The theoretical calculation using a small α value well represented the observations (Figs. 5, S1, and S2) and the Cole–Cole plots¹⁵ showed a semicircular shape (Fig. 6). These results indicate that slow magnetic relaxation occurs in a single process and **1** is regarded to be a field-induced SMM. The product of $\chi_T T$ was almost constant in this temperature range, and hence, χ_T obeys the Curie law below 8 K (Fig. S3). This is consistent with the dc susceptibility data, as well as zero-field ac data. Arrhenius analysis was carried out by using the estimated τ values, as shown in Fig. 7. A nonlinear plot was observed over the entire temperature range because of the presence of several relaxation processes. Relaxation may occur via direct and/or tunneling processes mainly at the low-temperature region, and via Raman and/or thermally assisted quantum tunneling relaxation of magnetization (TA-QTM) processes at the higher-temperature region.¹⁶ At high temperatures above 5 K, the plots measured under 1000 Oe dc field were almost linear. The data were thus analyzed on the basis of the Arrhenius law $\tau = \tau_0 \exp(\Delta E/k_B T)$. This gave the best fit parameters of $\Delta E/k_B = 35.7(6)$ K and $\tau_0 = 2.2(3) \times 10^{-7}$ s. The separation between the ground and first-excited sublevels of Ce(III) would be similar to this large E/k_B value, and the ground sublevels were solely populated below 10 K under these conditions. To reveal the detail of magnetic dynamics, the effects of a dc bias field on magnetic relaxation were confirmed from the field dependence of the ac susceptibility measured under several dc fields. Fig. 8 shows the dc field dependence of out-of-phase signals at 3 K measured under a field ranging from 20 Oe to 5000 Oe. The data well fitted the Debye model. Using the estimated relaxation time τ , the field dependence of the relaxation ratio τ^{-1} was confirmed (Fig. 9). The application of a weak dc field of up to 200 Oe resulted in the slowing down of the relaxation; however, application of a higher field enhanced τ^{-1} in a linear manner to the field. These observations can be correlated with the

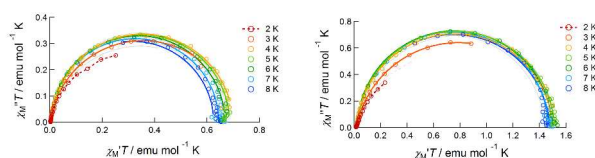


Fig. 6 Cole-Cole plots of **1** (left) and **3** (right) measured under an oscillating field of 3 Oe and an applied 1000 Oe dc field. Solid curves represent theoretical calculation on the basis of the generalized Debye model, whereas dashed curves are visual guides.

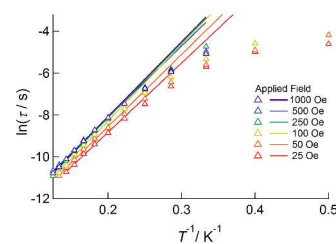


Fig. 7 Arrhenius plot for **1** measured under several applied dc fields. The solid lines represent the theoretical calculation based on the Arrhenius equation. For further detail, see the main text.

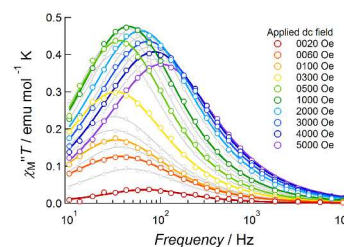


Fig. 8 Frequency dependence of products $\chi_M''T$ of **1** measured at 3.0 K under an oscillating field of 3 Oe and under several applied dc fields ranging from 20 Oe to 5000 Oe. Solid curves represent the theoretical calculations on the basis of the generalized Debye model.

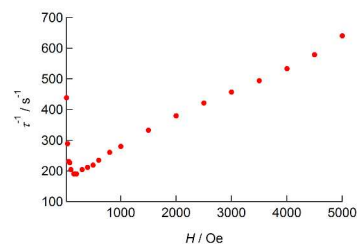


Fig. 9 Dc field dependence of the relaxation ratio τ^{-1} of **1** measured at 3.0 K.

resonance tunneling and direct processes, which are formulated below.¹⁶

$$\tau^{-1} = \frac{A_1}{1 + A_2 H^2} + B H^2 T + D \quad (1)$$

In eq. 1, the first and second terms denote the tunneling and direct processes, and the constant D includes the effect of other processes which are independent of the field at the given temperature. At a high field region where the tunneling relaxation is effectively suppressed, the direct process becomes dominant and would be enhanced in proportion to the square of

the magnitude of the field. This is not the case with the observations in Fig. 9. Hence, **1** does not obey Eq. 1. The field dependence of the relaxation was further confirmed over the whole temperature range with the field ranging from 25 to 1000 Oe. This is shown in Figs. 7 and S2. In Fig. S2, slight but continuous changes in the peak frequency are observed over the whole temperature range when the field is increased. In the Arrhenius plots, upon increasing the field, a gradual slowdown is observed for the whole temperature region. Above 500 Oe, τ^{-1} became independent of the field. To date, no explanation can be offered to explain such a strong field dependence of the relaxation ratio. However, we attended to the high-temperature region above 5 K, where all the plots were linear to $1/T$. The effective barrier $\Delta E/k_B$ estimated for each applied field coincided within the standard deviations [33(1)–36(1) K]. We assume that the Arrhenius analysis, which gave $\Delta E/k_B = 35.7(6)$ K under a 1000 Oe bias field, is effective even for **1**, and this value characterizes the SMM features of **1**.

Nd(III) complex **3** exhibited similar SMM features to those of **1** (Figs. 10, S4, and S5). Under zero field, no out-of-phase signals were observed. A weak bias field ranging from 25 Oe to 100 Oe invoked slow relaxation accompanied by weak signals of $\chi_M''T$. The intensity of $\chi_M''T$ increased and almost reached half the value of $\chi_T T$ when the bias field was increased to above 1000 Oe. This occurred along with the disappearance of $\chi_S T$. The amplitude of $\chi_M''T$ is very sensitive to the magnitude of a weak dc field similar to that of Ce(III)-based SMMs. The susceptibility data obeyed Debye relaxation and was fitted with the generalized Debye equations (Table S2). The small α parameters, as well as the semicircular Cole–Cole plots¹⁵ (Fig. 6), confirm that slow magnetic relaxation occurs via a single process. Thus, **3** can be regarded as a field-induced SMM. The product of $\chi_T T$ measured at 1000 Oe obeys the Curie law below 8.5 K (Fig. S6). This is consistent with the dc susceptibility data. The dynamic behavior of the magnetic relaxation was quantitatively analyzed using the Arrhenius plot. This again showed a strong dc field dependence and bending over the whole temperature range. Under a low dc field (below 50 Oe), relaxation ratio τ^{-1} was almost constant, and tunneling relaxation may occur under this condition. Upon increasing the dc field to 250 Oe, the relaxation ratio slowed down, while above 1000 Oe, it became independent of the field. Using the data above 5 K and under a 1000 Oe dc field, where the plot was almost linear, barrier $\Delta E/k_B$ and relaxation time τ_0 were estimated to be 38.5(5) K and $2.07(14) \times 10^{-7}$ s, respectively. The strong field dependence of **3** was rather strange and slightly different from that of **1**. We have tried to analyze these phenomena using equation 1, with no success. The slow magnetic relaxation of **3** and **1** was very complicated and did not obey the model previously reported. At a high field above 500 Oe and at a high-temperature region above 5 K, the Arrhenius plots were overlapping and the effect of the bias dc field might be negligible. The linear Arrhenius analysis in this temperature region is again effective to characterize the SMM features of the Nd(III)-based SMM.

Comparison of the SMM behavior of light lanthanide and heavy lanthanide complexes

The family of isostructural lanthanide complexes provides a unique opportunity to study magnetostructural correlations as they involve different lanthanide ions located in a similar coordination environment. In the previous paper, we have reported the SMM features of Tb(III) and Dy(III) complexes that

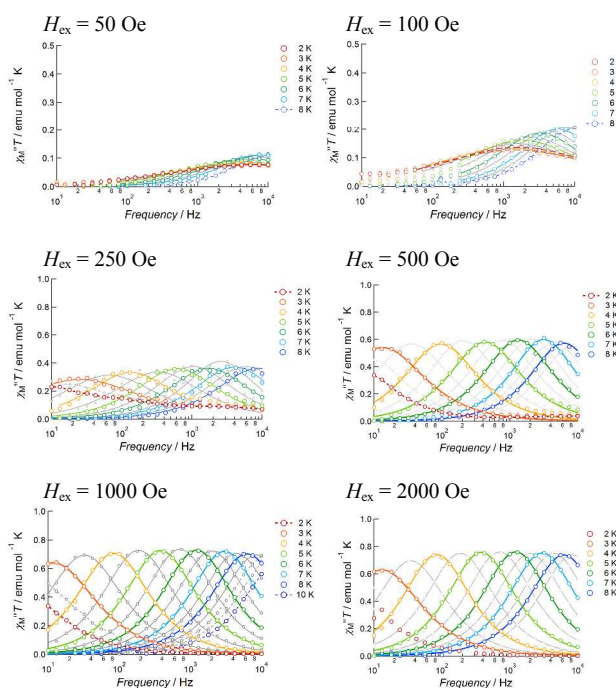


Fig. 10 Frequency dependence of products $\chi_M''T$ of **3** measured under an oscillating field of 3 Oe and an applied external dc field ranging from 25 Oe to 2000 Oe. Solid curves represent theoretical calculation on the basis of the generalized Debye model whereas dashed curves are visual guides.

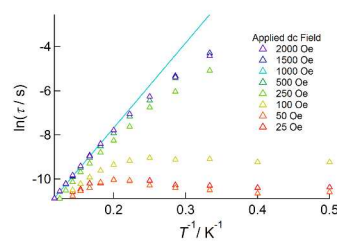


Fig. 11 Arrhenius plot for **3** measured under several applied dc fields. The solid line represents the theoretical calculation based on the Arrhenius equation.

were isostructural to complexes **1–4** reported here.^{3a} It had been reported that Ce(III), Pr(III), Nd(III), Tb(III), and Dy(III) ions are oblate-type ions, whose highest $|J_z|$ sublevels have oblate-shaped electronic distributions. A similar magnetic anisotropy can thus be expected in a similar anisotropic coordination environment. As was expected, most of these complexes behaved as SMMs; however, the magnetic relaxation behavior was slightly different between light and heavy lanthanide ions. The Tb(III) complex exhibited a field-induced SMM feature accompanied by fast quantum-tunneling relaxation under zero dc field conditions. On the other hand, the Dy(III) complex showed slow magnetic relaxation both under zero-field and applied dc field conditions. The difference in these complexes can be attributed to the parity of the total angular momentum J ; Tb(III) is known as a non-Kramers ion, which has a total angular momentum of 6, whereas Dy(III) is a Kramers ion with a J of 15/2. The rhombic anisotropic terms affect the mixing of ground and excited $|J_z|$ sublevels, especially in the case of non-Kramers ions. As a result, the Tb(III) complex exhibited fast

QTM relaxation that was avoided by applying a bias dc field with a strength of 1000 Oe. Light lanthanide complexes showed similar but slightly different trends of parity. The Ce(III) and Nd(III) complexes, as Kramers systems, behaved as field-induced SMMs, whereas the Pr(III) complex, as a non-Kramers system, was paramagnetic. Due to smaller J values for light lanthanide ions ($J = 5/2, 4,$ and $9/2$ for Ce(III), Pr(III), and Nd(III), respectively) compared with those of heavy lanthanide ions ($J = 6$ and $15/2$ for Tb(III) and Dy(III), respectively), we assumed that the magnitude for the mixing of $|J_z|$ sublevels might be larger for light lanthanide ions than for heavy lanthanide ions. As a result, QTM relaxation could be more enhanced for complexes with light lanthanide ions. Pr(III) as a non-Kramers ion is the most sensitive ion to rhombic anisotropy that mixes J_z sublevels via the \hat{J}_+ and \hat{J}_- operators related to the Stevens operator equivalents $\hat{O}_2^2, \hat{O}_4^4,$ and so on. This would lead to small separations among ground and excited sublevels that resulted in thermal depopulation even at low temperatures below 10 K. On the contrary, the mixing effects were smaller but not negligible in the Kramers ions Ce(III) and Nd(III). The separation among the ground and 1st excited J_z sublevels are large in these complexes ($\Delta E/k_B = 36.1(8)$ K and $38.5(5)$ K estimated from linear Arrhenius analysis). These obey Curie's law below 10 K. On the other hand, slight mixing of the ground J_z sublevels derives fast QTM relaxation under zero-field conditions. This was well prevented by applying a weak dc field above 500 Oe. The Sm(III) ion located at the border of the oblate and prolate ions did not exhibit any SMM features due to mismatching within the anisotropic coordination environment in complex 4.

Conclusions

In summary, we reported the synthesis of four isostructural Zn(II)–Ln(III)–Zn(II) trinuclear complexes that involve light lanthanide ions (Ln = Ce **1**, Pr **2**, Nd **3**, and Pr **4**) as magnetic centers. The dynamic behavior of their magnetic relaxation phenomena was investigated. The anisotropic coordination environment of each complex favors oblate lanthanide ions such as Ce(III), Pr(III), and Nd(III) to achieve a slow magnetic relaxation. To construct the Ce(III)- and Nd(III)-based SMMs, a synthetic strategy for the construction of Tb(III) and Dy(III) SMMs was useful due to the similarity of the electronic structures of these lanthanide ions. However, the resulting SMM features, especially dc field dependence, were rather different between light and heavy lanthanides. We have confirmed that the slow magnetic relaxation phenomena of light lanthanide SMMs were strongly dependent on the applied dc field and were controllable by the tuning of the strength of the external dc field.

Acknowledgements

This work was supported by a Grant-in Aid for Scientific Research (B) (no. 23350067) and Grant-in-Aid for Exploratory Research (no. 24655127) from JSPS Japan.

Notes and references

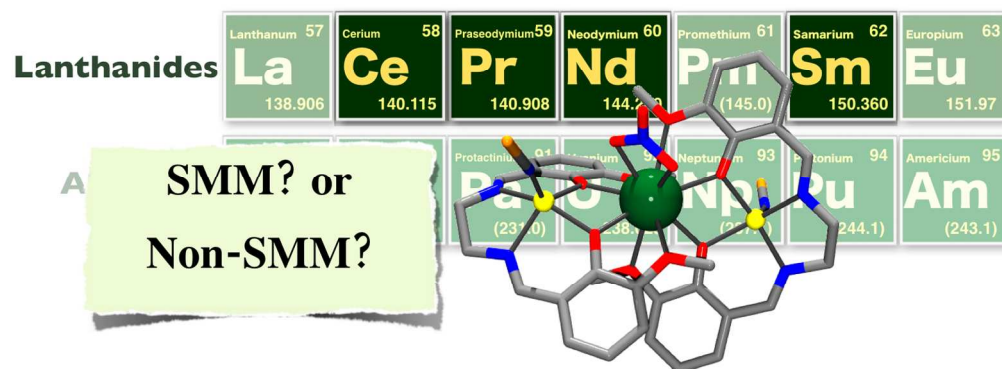
- a Faculty of Science, Nara Women's University, Nara, Nara 630-8506, Japan. Tel: +81-742-20-3402; E-mail: kajiwara@cc.nara-wu.ac.jp
 b Graduate School of Science, Osaka University, Toyonaka, Osaka 560-0043, Japan.

c Institute for Materials Research, Tohoku University, Aoba-ku, Sendai, Miyagi 980-8577, Japan.

† Electronic Supplementary Information (ESI) available: Additional magnetic data of the complexes. CCDC 1418301-1418304. See DOI: 10.1039/b000000x/

- (a) D. Gatteschi, R. Sessoli, and J. Villain, *Molecular Nanomagnets*, Oxford University Press, 2006; (b) T. Glaser, *Chem. Comm.* 2011, **47**, 116; (c) R. A. Layfield, *Organometallics* 2014, **33**, 1084; (d) R. Sessoli and A. K. Powell, *Coord. Chem. Rev.* 2009, **253**, 2328; (e) D. Gatteschi, *J. Alloys Compd.* 2001, **317-318**, 8; (f) N. T. Madhu, J.-K. Tang, I. J. Hewitt, R. Clérac, W. Wernsdorfer, J. van Slageren, C. E. Anson, and A. K. Powell, *Polyhedron* 2005, **24**, 2864.
- (a) P. Zhang, Y.-N. Guo, and J. Tang, *Coord. Chem. Rev.* 2013, **257**, 1728; (b) D. N. Woodruff, R. E. P. Winpenny, and R. A. Layfield, *Chem. Rev.* 2013, **113**, 5110; (c) H. L. C. Feltham and S. Brooker, *Coord. Chem. Rev.* 2014, **276**, 1; (d) Y.-N. Guo, G.-F. Xu, Y. Gao, and J. Tang, *Dalton Trans.* 2011, **40**, 9953.
- (a) P. L. Then, C. Takehara, Y. Kataoka, M. Nakano, T. Yamamura, and T. Kajiwara, *Dalton Trans.* submitted; (b) S. Hino, M. Maeda, Y. Kataoka, M. Nakano, T. Yamamura, and T. Kajiwara, *Chem. Lett.* 2013, **42**, 1276; (c) S. Hino, M. Maeda, K. Yamashita, Y. Kataoka, M. Nakano, T. Yamamura, H. Nojiri, M. Kofu, O. Yamamuro, and T. Kajiwara, *Dalton Trans.* 2013, **42**, 2683; (d) K. Yamashita, R. Miyazaki, Y. Kataoka, T. Nakanishi, Y. Hasegawa, M. Nakano, T. Yamamura, and T. Kajiwara, *Dalton Trans.* 2013, **42**, 1987; (e) M. Maeda, S. Hino, K. Yamashita, Y. Kataoka, M. Nakano, T. Yamamura, and T. Kajiwara, *Dalton Trans.* 2012, **41**, 13640; (f) A. Watanabe, A. Yamashita, M. Nakano, T. Yamamura, and T. Kajiwara, *Chem. Eur. J.* 2011, **17**, 7428; (g) A. Yamashita, A. Watanabe, S. Akine, T. Nabeshima, M. Nakano, T. Yamamura, and T. Kajiwara, *Angew. Chem. Int. Ed.* 2011, **50**, 4016; (h) T. Kajiwara, M. Nakano, K. Takahashi, S. Takaishi, and M. Yamashita, *Chem. Eur. J.* 2011, **17**, 196; (i) T. Kajiwara, M. Nakano, S. Takaishi, and M. Yamashita, *Inorg. Chem.* 2008, **47**, 8604.
- (a) S. Yamauchi, T. Fujinami, N. Matsumoto, N. Mochida, T. Ishida, Y. Sunatsuki, M. Watanabe, M. Tsuchimoto, C. Coletti, and N. Re, *Inorg. Chem.*, 2014, **53**, 5961; (b) F. Pointillart, K. Bernot, G. Poneti, and R. Sessoli, *Inorg. Chem.*, 2012, **51**, 12218; (c) S. K. Langley, N. F. Chilton, B. Moubaraki, and K. S. Murray, *Chem. Commun.*, 2013, **49**, 6965; (d) K. Ehama, Y. Ohmichi, S. Sakamoto, T. Fujinami, N. Matsumoto, N. Mochida, T. Ishida, Y. Sunatsuki, M. Tsuchimoto, and N. Re, *Inorg. Chem.*, 2013, **52**, 12828; (e) V. E. Campbell, R. Guillot, E. Riviere, P.-T. Brun, W. Wernsdorfer, and T. Mallah, *Inorg. Chem.*, 2013, **52**, 5194.
- (a) F. Pointillart, K. Bernot, R. Sessoli, and D. Gatteschi, *Chem. Eur. J.* 2007, **13**, 1602; (b) J. Ruiz, A. J. Mota, A. Rodríguez-Diéguez, S. Titos, J. M. Herrera, E. Ruiz, E. Cremades, J. P. Costes, and E. Colacio, *Chem. Commun.* 2012, **48**, 7916.
- J.-L. Liu, Y.-C. Chen, Y.-Z. Zheng, W.-Q. Lin, L. Ungur, W. Wernsdorfer, L. F. Chibotaru, and M.-L. Tong, *Chem. Sci.* 2013, **4**, 3310.
- (a) N. Ishikawa, M. Sugita, T. Ishikawa, S.-y. Koshihara, and Y. Kaizu, *J. Phys. Chem. B* 2004, **108**, 11265; (b) M. Gonidec, R. Biagi, V. Corradini, F. Moro, V. De Renzi, U. del Pennino, D. Summa, L. Muccioli, C. Zannoni, D. B. Amabilino, and J. Veciana,

- J. Am. Chem. Soc.* 2011, **133**, 6603; (c) C. R. Ganivet, B. Ballesteros, G. de la Torre, J. M. Clemente-Juan, E. Coronado, and T. Torres, *Chem. Eur. J.* 2013, **19**, 1457.
- 8 N. Ishikawa, M. Sugita, T. Ishikawa, S.-y. Koshihara, Y. Kaizu, *J. Am. Chem. Soc.* 2003, **125**, 8694.
- 9 (a) S. Demir, J. M. Zadrozny, and J. R. Long, *Chem. Eur. J.*, 2014, **20**, 9524; (b) F. Tuna, C. A. Smith, M. Bodensteiner, L. Ungur, L. F. Chibotaru, E. J. L. McInnes, R. E. P. Winpenny, D. Collison, and R. A. Layfield, *Angew. Chem. Int. Ed.* 2012, **51**, 6976; (c) L. Ungur, J. J. Le Roy, I. Korobkov, M. Murugesu, and L. F. Chibotaru, *Angew. Chem. Int. Ed.* 2014, **53**, 4413; (d) M.-E. Boulon, G. Cucinotta, S.-S. Liu, S.-D. Jiang, L. Ungur, L. F. Chibotaru, S. Gao, and R. Sessoli, *Chem. Eur. J.* 2013, **19**, 13726.
- 10 (a) J. D. Rinehart and J. R. Long, *Dalton Trans.* 2012, **41**, 13572; (b) J. J. Le Roy, I. Korobkov, J. E. Kim, E. J. Schelter and M. Murugesu, *Dalton Trans.* 2014, **43**, 2737; (c) J. J. Baldoví, J. M. Clemente-Juan, E. Coronado, Y. Duan, A. Gaita-Ariño, and C. Giménez-Saiz, *Inorg. Chem.* 2014, **53**, 9976; (d) S. K. Singh, T. Gupta, L. Ungur, and G. Rajaraman, *Chem. Eur. J.* 2015, **21**, DOI: 10.1002/chem.201501330.
- 11 (a) D. Schmitt, *J. Phys.* 1986, **47**, 677; U. Walter, *Z. Phys. B: Condens. Matter* 1986, **62**, 299; (b) J. Sievers, *Z. Phys. B: Condens. Matter Quanta* 1982, **45**, 289.
- 12 J. R. Rinehart and J. R. Long, *Chem. Sci.*, 2011, **2**, 2078.
- 13 (a) *Crystal Clear; version 1.3.5; Operating software for the CCD detector system*, Rigaku and Molecular Structure Corp., Tokyo, Japan and The Woodlands, Texas, 2003; (b) A. Altomare, M. C. Burla, M. Camalli, G. L. Casciarano, C. Giacovazzo, A. Guagliardi, A. G. G. Moliterni, G. Polidori, and R. J. Spagna, *Appl. Cryst.* 1999, **32**, 115; (c) G. M. Sheldrick, *SHELXL-97: Program for the Refinement of Crystal Structures*. University of Göttingen, Göttingen, Germany, 1996.
- 14 S. Zhao, X. Lü, A. Hou, W.-Y. Wong, W.-K. Wong, X. Yang, R. A. Jones, *Dalton Trans.*, 2009, **38**, 9595.
- 15 K. S. Cole and R. H. Cole, *J. Chem. Phys.*, 1941, **9**, 34.
- 16 (a) A. Abragam and B. Bleaney, *Electron Paramagnetic Resonance of Transition Ions*, Oxford University Press, 1970; R. L. Carlin, *Magnetochemistry*, Springer-Verlag, 1986; (b) A. Singh and K. N. Shrivastava, *Phys. Status Solidi B*, 1979, **95**, 273; (c) K. N. Shrivastava, *Phys. Status Solidi B*, 1983, **117**, 437.
- 17 J. M. Zadrozny, M. Atanasov, A. M. Bryan, C.-Y. Lin, B. D. Rekker, P. P. Power, F. Neese, and J. R. Long, *Chem. Sci.*, 2013, **4**, 125.
- 18 S.-D. Jiang, B.-W. Wang, G. Su, Z.-M. Wang, S. Gao, *Angew. Chem. Int. Ed.* 2010, **49**, 7448.



Four isostructural Zn(II)-Ln(III)-Zn(II) trinuclear complexes were synthesized using light lanthanide ions as magnetic centers, of which Ce(III) and Nd(III) complexes behaved as single-molecule magnets.
574x245mm (72 x 72 DPI)